Proceedings of the 21st ICSMGE, Vienna, Austria, 14 – 19 June 2026. Pistrol, Adam & Schweiger (eds.)
Published by: ÖGG, Austrian Society for Geomechanics, Salzburg, Austria, ISBN 978-3-9503898-4-5
https://doi.org/10.53243/ICSMGE2026-2041

A novel approach using shrinkage curves for predicting sensitivity to hydraulic and structural property changes due to cyclic wetting-drying

Lorenz Spillecke, Alexander Knut, Ralf Thiele, Antje Bornschein
Institute of Geotechnics Leipzig, UAS Leipzig, Germany, lorenz.spillecke@htwk-leipzig.de

ABSTRACT: Understanding the effects of cyclic wetting and drying on hydraulic conductivity and structural changes in soils is essential for ensuring the long-term stability of hydraulic barriers. This study explores a novel approach to predict the cyclic behaviour of soil properties by utilizing shrinkage curves. The method, which employs optical volume measurements, replaces an otherwise time-consuming process that measures the hydraulic conductivities throughout wetting-drying cycles. Additionally, the incorporation of shrinkage curves, in combination with cyclic hydraulic properties, provides further insights into soil-specific behaviour. Shrinkage curves were obtained by measuring volume changes of five distinct soil compositions using a laser scanner and camera. Unlike traditional methods, which rely on labour-intensive, manual, and sometimes destructive volume measurements, the optical method continuously and accurately captures the volume change of the shrinking soil samples. The shrinkage curve was correlated with measurements of hydraulic conductivity before and after 5 wetting drying cycles to establish relationships between shrinkage behaviour and hydraulic properties. Key parameters derived from shrinkage curves, such as the shrinkage ratio and shrinkage rate, were employed to predict the soil's sensitivity to dynamic structural and hydraulic changes caused by wetting-drying cycles. This study demonstrates that structural changes, including variation of density and hydraulic properties due to cyclic moisture fluctuations, can be estimated using the proposed method, to prevent the need for time-consuming wetting-drying experiments. By integrating advanced techniques, such as optical volume measurement, the study establishes a more reliable framework for evaluating soil specific behaviour. The shrinkage curve is introduced as a practical tool for characterizing soil behaviour under cyclic conditions. These contributions significantly enhance the understanding of soil dynamics for improving the design, sustainability and resilience of hydraulic barriers such as embankment sealing layers.

KEYWORDS: hydraulic conductivity, unsaturated soil, optical volume measurement, soil shrinkage curve, cyclic wetting drying

1 INTRODUCTION

Earthen sealing layers, such as in levee constructions, form a primary barrier against uncontrolled seepage. Projected climate-change scenarios for Central Europe and many other regions are characterized by prolonged, hotter dry periods alternating with intense rainfall events. Consequently, these barriers are exposed to more frequent and more extreme wetting–drying (W–D) cycles, even when overlying protection layers are in place (Puppala et al 2009, Janga et al 2024).

W–D cycling alters the fabric and pore network of cohesive soils, producing measurable changes in both mechanical (Cuisinier et al. 2020, Tang et al. 2021) and hydraulic behaviour (Abbas et al. 2023, Louati et al. 2018, Malusis et al. 2011). Laboratory studies have documented increases in saturated hydraulic conductivity by one to two orders of magnitude (i.e. 10- to 100-fold), and in some cases by as much as 1000-fold, after only a few cycles (Lin 2000, Rao et al. 2000, Lu et al. 2015, Louati et al. 2018 and Camillis et al. 2019).

The underlying mechanisms are progressive aggregate loosening, micro-cracking and the attendant reduction in bulk density (Louati et al. 2018, Ivoke et al 2021, Han et al 2022 and Abbas et al 2023). These are influenced by soil specific factors like the initial soil structure (Zhou et al 2012, Estabragh et al 2015 and Abbas et al 2023) and mineralogy (Han et al 2022, Tang et al 2021) as well as environmental and external factors like root growth or the current stress state of the soil (Tang et al 2021).

Current design specifications for mineral sealing layers are based on a maximum hydraulic conductivity, typically $k_f \leq 1 * 10^{-7} m * s^{-1}$ and a target compaction level e.g. $D_{Pr} \geq 97\%$ of Standard Proctor (DWA-M 512-1 2012). Such limit values implicitly assume that material properties remain constant over the service life of the structure. To move toward performance-based design, test methods are required that capture the dynamic response of sealing soils to alternating hydrological loads.

As the evaluation of cyclic W-D changes on hydraulic properties is time-consuming, the suitability of simple index values for estimation of the sensitivity of a distinct soil structure needs to be evaluated. Volumetric shrinkage integrates key phenomena such as structural changes, crack generation, and density loss and therefore might be closely linked to effects eminent during W-D cycles (Coppola et al. 2012).

While the conventional shrinkage-limit test delivers only a single index value, modern optical methods can trace the entire soil-shrinkage curve (SSC) with sub-millimetre resolution and thus offer a far richer data set for material qualification (Sander & Gerke 2007, Amenuvor et al. 2020, Jain & Wang 2015; Henke et al. 2023; Wong et al. 2019 and Sharanya et al. 2021).

In this study, potential metrics of the SSC were evaluated as an assessment tool to predict the sensitivity of fine-grained soils suitable as surface barrier material regarding saturated hydraulic conductivity changes resulting from multiple W-D cycles.

1.1 *Shrinkage limit – concept, assumptions and pitfalls*

The transition from a semi-solid to a solid consistency is defined as the shrinkage limit. The determination of the shrinkage limit is specified in various standards (DIN EN 18122-2, ASTM 4943-18, BS 1337). At water contents below this limit, no further bulk-volume loss is expected, even though drying continues. In standard practice the shrinkage limit is calculated from the final dry mass m_d and the volume V_d ,which is assumed to have remained fully saturated until shrinkage limit. According to (Schultze et al. 1967, DIN 18122-2) the shrinkage limit is calculated as follows:

$$w_s = \left(\frac{V_d}{m_d} - \frac{1}{\varrho_s} \right) \cdot \varrho_w \cdot 100 \quad (1)$$

where V_d and m_d are the volume and the mass of the dry sample and ϱ_s and ϱ_w are the particle density and the density of water respectively. In contrast to DIN 18122-2 the shrinkage limit according to ASTM D4943-18 is calculated as follows:

$$SL = w - \left(\frac{V - V_d}{m_d}\varrho_w\right) \cdot 100 \quad (2)$$

where w is the initial water content after the sample preparation. V and V_d are the initial volume and the volume of the dry sample after shrinkage and oven drying.

The estimation of the shrinkage limit according to (1) and (2) considers only linear shrinkage and dismisses the effects of the structural, residual and zero shrinkage phase (Vogt et al. 2013, Spillecke et al. 2025) leading to an overestimation of the shrinkage limit with water contents that even exceed the plastic limit (DIN 18122-2, Spillecke et al. 2025).

1.2 *The soil-shrinkage curve (SSC) as a comprehensive descriptor*

A more informative approach traces the complete soil-shrinkage curve, plotting void ratio e against moisture ratio ϑ throughout drying. Empirically the curve exhibits up to four regimes, the structural, linear, residual and zero shrinkage (Peng & Horn 2013). The structural shrinkage is the initial shrinkage phase, characterized by a reduction in moisture ratio with little structural changes. Within the linear shrinkage, mostly pore water evaporates whereas a constant gradient of the shrinkage curve is expected. During the residual phase, the shrinkage rate declines while mainly hygroscopic water dries subsequently (Mitchell 1991). The zero-shrinkage phase is characterized by a neglecting volumetric change due to further desiccation. Shrinkage curves with up to six distinct combinations (Type A-F) of these regimes are documented (Peng & Horn 2013).

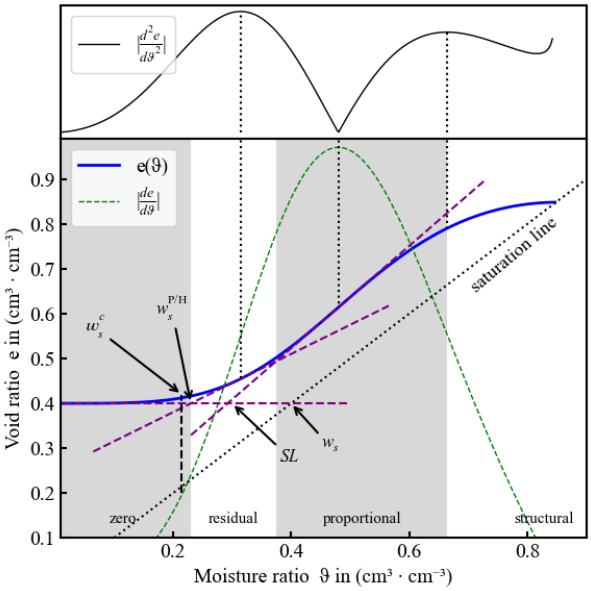

Figure 1 Theoretical shrinkage curve including phase derivation

To describe the shrinkage curve, a model which is using the inverse of the van Genuchten equation (Genuchten 1980), commonly used for the modelling of the soil water retention curve, was adapted by Peng & Horn (2007):

$$e(\upsilon) = e_r + \frac{e_s - e_r}{\left(1 + \left(\frac{\alpha \cdot \vartheta}{e_s - \vartheta}\right)^{-n}\right)^{m}} \quad (4)$$

Within this e_r and e_s are the residual and saturated void ratio and α, m and n are fitting parameters. By evaluating the first and second derivatives of this function, the inflection points that delimit the shrinkage regimes can be located objectively, and a model-based shrinkage limit $w_s^{P/H}$ can be defined at the beginning of the zero-shrinkage phase (Figure 1). The shrinkage limit estimated with the model-based approach is consistently lower and more in line with the definition of the shrinkage limit than the value obtained from the conventional formula (Spillecke et al. 2025).

$$w_s^c := \left\{\vartheta \;\middle|\; \left|\frac{de}{d\vartheta}\right| = 0{,}2\right\} \quad (3)$$

For comparison, different exemplary results are put together in Figure 1. The disparity between the different approaches is evident. The extend of structural shrinkage and the curvature in the residual phase largely determine the magnitude of the error between methods. (1). In this study, an alternative shrinkage limit w_s^c was defined as the point at which the shrinkage rate drops below a constant threshold of 0.2. The superscript "c" denotes the use of a constant threshold criterion:

1.3 *Wet–dry cycling and implications for levee performance*

Previous studies show that several W-D cycles can raise saturated hydraulic conductivity by one to two orders of magnitude and shift the unsaturated conductivity curve upward across the wet–dry range (Spillecke et al. 2025). Dense, highly compacted specimens tend to loosen as fissures reopen and aggregate fabric relaxes, whereas initially loose specimens densify (Louati et al. 2018 and Spillecke et al. 2025).

Design values for saturated hydraulic conductivity (k_f) and target dry densities ($D_{Pr,97}$) derived from static laboratory tests cannot guarantee long-term sealing if the soil alternates its properties under cyclic moisture stress. In practice, this means that levee designs predicated solely on a single k_f value or a Proctor density risk underestimating the degradation in barrier performance over a structure's service life. Currently, there are no standard test procedures to predict sensitivity of hydraulic conductivity changes due to climatic alteration.

2 MATERIAL AND SAMPLE PREPARATION

The research utilized four lean clays (CL), one silty clay (CL-ML) and one silt (ML), all categorically allowed for surface barrier applications in levee infrastructure. In accordance with DIN 18122-2 standards, particles exceeding 0.5 mm were removed prior to testing. Six natural soils were selected with slight variations in clay and sand content. These soils are devoid of organic material. A summary of the tested materials is provided in Table 1. The corresponding particle size distribution is shown in figure 2.

The Atterberg limits were determined following DIN EN ISO 17892-12 standards. The shrinkage limit was measured in accordance with DIN 18122-2, utilizing the calliper method to assess the volume of the dry sample. Particle densities were assumed at 2.68 Mg/m³.

For specimen preparation, the samples were oven dried, grinded and distilled water amounting to 1.1 times the liquid limit (LL) was added to achieve the prescribed remoulding moisture content. Samples were cast into acrylic-glass rings

Table 1: sample compositions and classification

	Soil D	Soil A	Soil B	Soil E	Soil C	Soil F
LL[+]	22.7	24.4	29	27.8	23.7	33.8
PL[#]	15.5	12.2	12.6	16.7	18.3	23.9
w_s	14.1	13.9	10.9	15.1	19.2	21.1
SL	9.7	9.1	9.5	10.5	16.9	19.6
PI[†]	7.2	10.2	16.4	11.1	5.4	9.9
USCS[*]	CL	CL	CL	CL	CL-ML	ML

[+]Liquid limit in (%), [#]Plastic limit in (%), [†]Plasticity index in (%), [*]Unified Soil Classification System

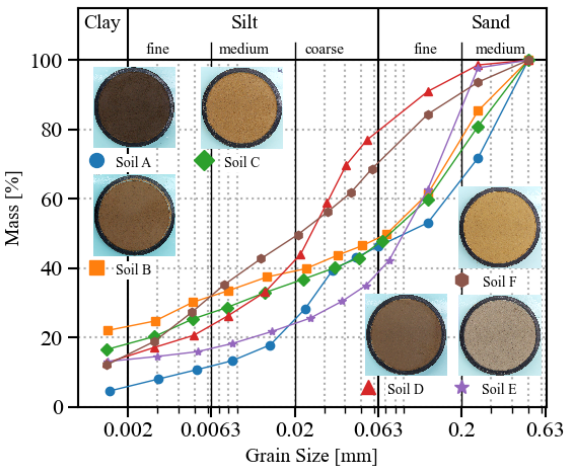

Figure 2 Particle size distribution of all 6 distinct soil samples. Grain size > 0.5 mm was removed before

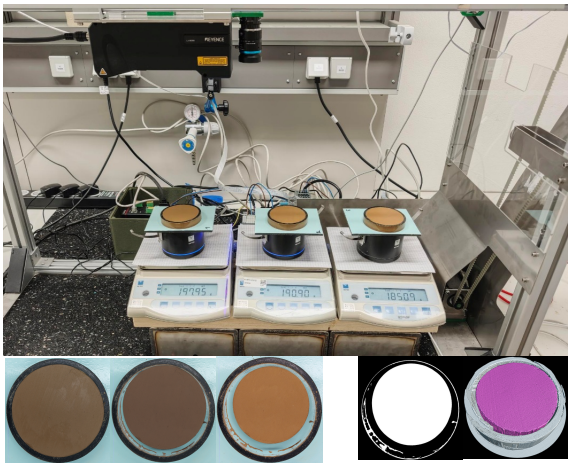

Figure 3 Top - Experimental setup with Laser and camera above the soil samples, Bottom - image of a sample at beginning, after 24 hours and after 48 hours – right thresholded image and 3d model

with an internal diameter of 70 mm and a height of 14 mm, positioned on an acrylic plate. To facilitate image processing, the ring faces were pre-wrapped with black film, and the plate was wrapped with blue film. Initial mass and geometric dimensions were recorded, and specimens were centrally positioned on balances directly beneath a fixed camera-laser assembly for measurement.

3 METHOD

3.1 *Soil Shrinkage Curve determination*

During the desiccation process, digital imagery was continuously captured at 30-minute intervals. The imaging apparatus utilized was a Raspberry Pi camera featuring a 1/2.3-inch sensor, 12-megapixels resolution and a 16 mm telephoto lens, chosen explicitly to reduce optical distortions. All images were taken under uniform, diffuse lighting conditions within a shaded environment. Surface topography was analysed using a 2D laser profilometer (Keyence LJ-X8300), offering a planar resolution of 0.1 mm and a vertical resolution of 3 µm. Mass measurements were automatically recorded every 10 minutes using the HYPROP-2 balance. The ambient temperature was consistently maintained at 22°C. The experiment was discontinued once no significant mass change was observed, typically after 3 to 4 days, with the specimens retaining approximately 2% residual moisture by weight. Subsequently, the specimens were oven-dried at 60°C until reaching a constant mass. The residual volume was assessed by another laser scan and a calliper measurement for validation purpose.

For the estimation of the SSC, it is necessary to determine the sample volume during the shrinkage process. For each specimen, the complete sequence of digital images was imported into ImageJ and separated into hue, saturation, and brightness components. Pixels located outside the inner boundary of the sample ring were masked (see figure 3). The hue component was utilized for threshold-based segmentation due to its high contrast between the soil chroma and the blue pad. A region-growing-algorithm utilizing the implemented "wand" tool was applied to measure the areas of an image sequence in a batch process.

The sample area in object coordinates (pixels) was identified for each acquisition segmentation. Subsequently, these areas were converted into world coordinates (millimeters) using the following transformation formula:

$$A_{obj,i} = k\, A_{img,i} \tag{5}$$

where $A_{obj,i}$ and $A_{img,i}$ are the areas in object and image coordinates, and k is a constant scaling factor determined by an object of known dimensions.

For sample height determination, the point cloud data, which was obtained by the 2D-laser scanner was used. Within the point cloud, a circular grid was established on top of the sample. Within the grid, a median point height was scaled to world coordinates by utilising the known ring height, similar as in the method used for area measurements, described in equation (5). A 3D reconstruction of the sample as displayed in figure 3 was used for further validation. The following formula, which implies the height and area measurements underpins the volume and therefore void ratio basis.

$$V_i = A_{obj,i} * \left(h_0 - \tilde{h}_{min,i}\right) \tag{6}$$

h_0 is the reference height of the sample ring and $\tilde{h}_{min}$ is estimated by the median of the height points on top of the sample. By this an even sample thickness of the whole specimen is assumed. This was confirmed by the last measurement, where the sample was turned upside down. The void ratio is estimated by:

$$e_i = V_i \frac{\varrho_s}{m_d} - 1 \tag{7}$$

The time-resolved volumes were paired with the corresponding mass change of the samples $\Delta\, m_i$ to construct shrinkage curves in the $\vartheta - e$ space, whereas the moisture ratio is defined as:

$$\vartheta_i = \frac{V_{w,i}}{V_s} = \frac{\varrho_s \left(m_{f,0} - \Delta\, m_i\right)}{\varrho_w\, m_d} \tag{8}$$

Within (8) a constant density of the pore water with ϱ_w = 1 g/cm³ is assumed. The initial dry and wet mass m_d, m_w are known due to the sample preparation.

3.2 *Saturated hydraulic conductivity: Sample preparation and W-D cycles*

Samples were prepared in 250 ml cylinders at optimal water content, with multilayer compaction to 97% of Proctor density, following the design criteria from DWA-M 512-1 2012.

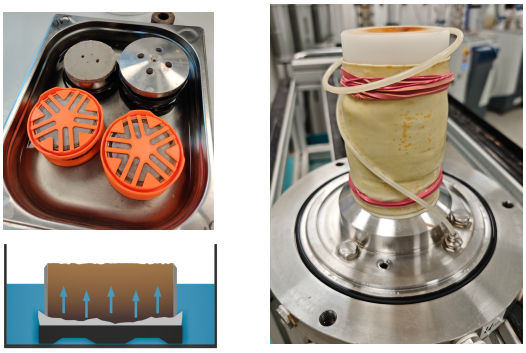

Figure 4 Top left – saturation method by capillary suction, Bottom left – schematic display of saturation method, Right – prepared sample for hydraulic conductivity measurement in triaxial cell

Samples were saturated by capillary suction in a basin. Capillary saturation was assumed to be finished after the change rate fell below 0,5 g per day. It is known that a saturation by capillary suction may not fully saturate the sample (Kutter 2012). Following the hypothesis that most addressed property changes occur at water contents above the air entry point (Yan et al. 2022), it was assumed, that achieving full saturation may not be essential.

After each drying cycle, samples were re-saturated following the same procedure, aiming for a non-destructive process repeated for five cycles. Hydraulic conductivity was measured in a triaxial cell based on DIN EN ISO 17892-11 2021. The backpressure necessary to provoke a full saturation was 800 kPa and the hydraulic gradient was chosen equally for all samples at i = 20. Separate samples were used for measurements after preparation and after five W-D cycles, as the process of backpressure saturation can alter sample structure.

4 RESULTS

Figure 5 (a) illustrates the various shrinkage data obtained by using the specified methodology in section 3.1. The dashed line indicates a full saturation. The data points are reduced for illustration purposes. Each curve is accompanied by its corresponding model fit, as defined by equation 2. The used fitting parameters are summarized in table 2.

According to Peng & Horn (2013) soil B, D and E exhibit all four phases of shrinkage (type A), whereas soil A lacks a distinct zero-shrinkage phase (type B) and soils C and F do not exhibit the structural shrinkage phase (type F). Additionally, the linear shrinkage phase for soil E surpasses the gradient of the saturation line. This may occur due to the collapse of structural pores following the sample preparation or potential measurement inaccuracies, which warrant further investigation.

For each soil the model proposed by (Peng & Horn 2007) referenced in Eq. (2) was used for the determination of the shrinkage regimes described in section 1.2. The shrinkage limit evaluated with the model-based approach $w_s^{P/H}$ as well as the one estimated with a simplified method w_s^c are summarized in table 2. In comparison with the evaluation proposed in the international standards, it is apparent that the model-based approach estimates accurately for SSC type A with respect to the shrinkage limit, as given in Eq. (2). Especially for SSC type B, which lacks the zero-shrinkage phase, the model-based approach overestimates the shrinkage limit dramatically, whereas a lack of the structural shrinkage phase leads to a slight underestimation. In contrast to this, the evaluation of the shrinkage ratio following Eq. (3) is more robust for SSC type C and F.

Table 2 Summarized results and used Fitting parameters related to eq. (2)

Soil	SSC	α	m	n	e_s	e_r	k_f^0	k_f^5	Δk_f^{W-D}	R	V_s	$w_s^{P/H}$	w_s^c	Δw_{res}
	Type	(-)	(-)	(-)	(-)	(-)	(m/s)	(m/s)	(m/s)	(%)	(%)	(%)	(%)	(%)
A	B	0.311	0.119	7.583	0.689	0.381	2.2E-09	4.2E-07	1.9E+02	1.950	22.25	14,59	1.30	14.00
B	A	0.463	0.486	3.022	0.776	0.377	1.5E-09	2.2E-07	1.5E+02	1.960	28.99	9,79	5.78	6.83
C	F	1.173	2.170	1.421	0.771	0.295	4.2E-10	5.3E-08	1.3E+02	2.080	36.56	7,14	6.26	6.31
D	A	0.456	0.544	3.595	0.816	0.408	3.6E-09	1.5E-07	4.2E+01	1.920	29.01	12,80	9.25	5.50
E	A	0.297	0.521	3.597	0.799	0.519	2.3E-09	5.1E-08	2.2E+01	1.770	17.65	16,07	13.63	4.96
F	F	1.967	12.850	1.677	0.985	0.570	2.0E-08	7.1E-08	3.6E+00	1.720	26.20	18,65	17.78	4.75

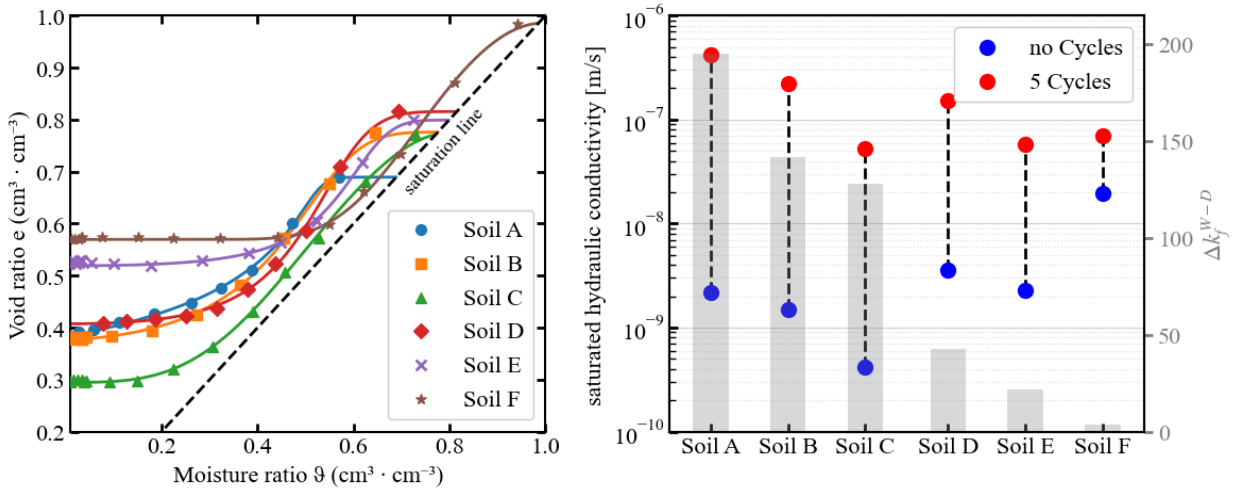

(a) (b)

Figure 5 The SSC of 6 distinguished soil samples (a) and the saturated hydraulic conductivity measured without and after five W-D cycles (b). The bar plot indicates the sensitivity of the soil changing its hydraulic conductivity due to W-D cycles as defined in eq. (3).

For further discussion of the results, the width of the residual shrinkage phase Δw_{res} (see Figure 1) interpreted as gravimetric water content is used. Additionally, the plasticity index, which can roughly be interpreted as the width of the linear shrinkage phase is used. Furthermore, the shrinkage ratio R and the volumetric shrinkage V_s, as defined in ASTM D4943, are discussed.

Figure 5 (b) illustrates the measured saturated hydraulic conductivities across different soil samples. Within this k_f^0 and k_f^5 are the initial hydraulic conductivity and the hydraulic conductivity after five W-D cycles respectively. Initially, each soil exhibits a lower hydraulic conductivity compared to values obtained after five consecutive W-D cycles. Notably, the magnitude of change varies significantly among the soils, with soil F establishing a 3.6-fold increase, whereas soil D demonstrates an almost 200-fold increase. To quantify the sensitivity of a particular soil to changes in its hydraulic conductivity due to W-D cycles, the following metric is used:

$$\Delta k_f^{W-D} = \frac{k_f^5}{k_f^0} \tag{9}$$

The metric proposed in (9) quantifies the absolute change in hydraulic conductivity with respect to k_f^0. The results summarized in table 2 are sorted with respect to (9) in descending order.

5 DISCUSSION

Figure 6 provides a comparative summary of the parameters documented in table 2 in relation to the observed hydraulic conductivity change factor shown in Eq. (8). The graph is used to make linear dependencies apparent. All curves are normalized to its respective maximum value.

The initial goal was to employ basic soil classification parameters as prediction tool for huge Δk_f^{W-D} changes. The volumetric shrinkage V_s and shrinkage ratio R both don't correlate with Δk_f^{W-D}. The conventional shrinkage limits used in standards and referenced in Eq. (1) and (2) as well as the shrinkage limit derived by the model-based approach $w_s^{P/H}$ are also not applicable as a predictor. Although the shrinkage limit decreases as Δk_f^{W-D} increases, they show little variance or even increase towards the highest Δk_f^{W-D} values. Furthermore, w_s is higher than the SL, and for soils A and C, these values are above the plastic limit.

The plasticity index PI shows similar trends as V_s and R. The PI is usually associated with the linear shrinkage phase, which does not appear to be significant for the change in hydraulic conductivity.

Also, parameters derived by the particle size distribution do not display a meaningful relationship with the observed variations in sensitivity to W-D cycles which is also known for the correlation with the shrinkage limit itself (Izdebska-Mucha et al 2013). The results so far confirm that the conventional classification tests provide limited predictive capability regarding the sensitivity of soils to hydraulic and structural degradation during cyclic wetting–drying loading.

A more promising correlation was recognised with the parameters w_s^c and Δw_{res} which show potential as a predictor. In particular w_s^c shows an inverse linear trend, while the width of the residual shrinkage phase Δw_s establishes linear or slight exponential trends (Figure 5). With these two parameters which mainly describe the size of the zero and residual shrinkage phase, it becomes likely that changes leading to higher Δk_f^{W-D} take place within these phases.

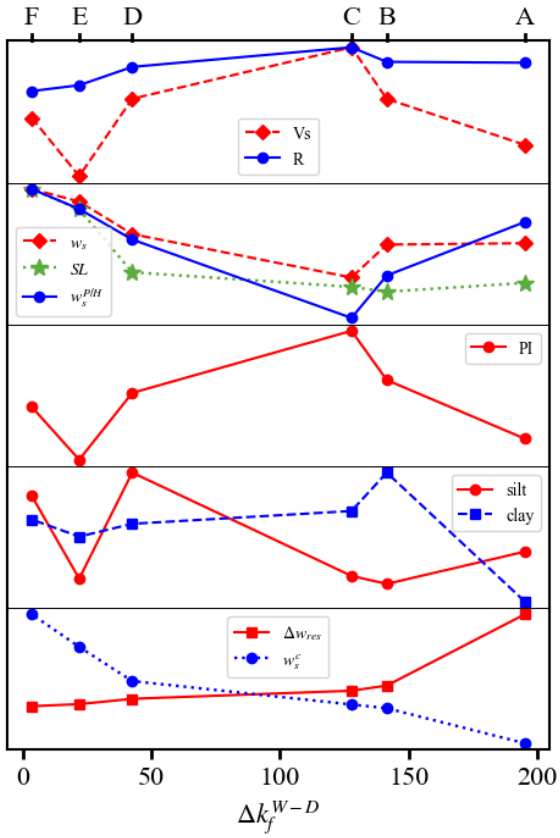

Figure 6 Correlation graph of the 6 soil samples, sorted and scaled to its kf-Value change under W-D cyclic stress. Curves are normalized to its maximum value.

This observation is consistent with previous studies, which emphasize that hydraulic response under cyclic moisture stress is largely governed by internal structural rearrangements and micro-cracking, which cannot be described by the conventional soil indices (Albrecht et al. 2001 and Romero et al. 2008). Further research is necessary to evaluate the dominant phenomena causing the change of hydraulic conductivity during the residual shrinkage phase.

6 CONCLUSIONS

This study proposes a novel, performance-oriented approach for assessing soil susceptibility to structural and hydraulic degradation under cyclic wetting–drying conditions. By employing an optical shrinkage curve analysis in place of conventional, time-intensive hydraulic testing, the proposed approach enables a more efficient evaluation of soil behaviour.

- Hydraulic conductivity testing demonstrates that W–D cycling can cause significant changes in barrier performance, with increases up to nearly 200-fold (Soil D, Figure 3). This leads to the fact that three of the six soils exceeded the design criteria of $k_f \leq 10^{-7}\ ms^{-1}$ after five cycles.
- Traditional classification parameters derived by the particle size distribution or the Atterberg limits do not reliably predict the extent of degradation of the hydraulic conductivity after cyclic W-D loading.
- In contrast, parameters derived from the soil-shrinkage curve, specifically the shrinkage limit at w_s^c and the width of the residual shrinkage phase, exhibit clear trends with the observed increases in saturated hydraulic conductivity.

Current static design standards are inadequate for guaranteeing the long-term integrity of sealing systems under recurring W-D conditions. Shrinkage curve analysis provides an approach to connect volumetric changes during dry out to structural changes within the soil matrix.

In summary, the results support the use of shrinkage curve analysis as a possible approach for assessing cyclic sensitivity, opposed to traditional index tests. By correlating the residual shrinkage phase width with post-cycling hydraulic conductivity, the estimation of the SSC may offer a quick, non-invasive way to assess the long-term integrity of barriers while, further research is needed to better understand the decisive mechanisms that influence the change of hydraulic permeability during shrinkage, especially in the residual phase.

7 REFERENCES

Abbas, M. F., Shaker, A. A., Al-Shamrani, M. A. 2023. Hydraulic and volume change behaviors of compacted highly expansive soil under cyclic wetting and drying. Journal of Rock Mechanics and Geotechnical Engineering. https://doi.org/10.1016/j.jrmge.2022.05.015

Albrecht, B. A., Benson, C. H. 2001. Effect of desiccation on compacted natural clays. Journal of Geotechnical and Geoenvironmental Engineering, 127(1), 67–75. https://doi.org/10.1061/(ASCE)1090-0241(2001)127:1(67)

Amenuvor, A. C., Li, G., Wu, J., Hou, Y., Chen, W. 2020. An image-based method for quick measurement of the soil shrinkage characteristics curve of soil slurry. Geoderma, 354, 114165. https://doi.org/10.1016/j.geoderma.2019.114165

Coppola, A., Gerke, H. H., Comegna, A., Basile, A., Comegna, V. 2012. Dual-permeability model for flow in shrinking soil with dominant horizontal deformation. Water Resources Research, 48, W08527. https://doi.org/10.1029/2011WR011376

Cuisinier, O., Masrouri, F., Mehenni, A. 2020. Alteration of the hydromechanical performances of a stabilized compacted soil. Journal of Materials in Civil Engineering, 32(11), 04020357. https://doi.org/10.1061/(ASCE)MT.1943-5533.0003270

De Camillis, M., Di Emidio, G., Bezuijen, A., Verastegui-Flores, R. D. 2019. Hydraulic conductivity of modified bentonites after wet and dry cycles. https://doi.org/10.1007/978-981-13-2224-2_58

Estabragh, A. R., Parsaei, B., Javadi, A. A. 2015. Laboratory investigation of the effect of cyclic wetting and drying on the behaviour of an expansive soil. Soils and Foundations, 55(2), 304–314. https://doi.org/10.1016/j.sandf.2015.02.007

Han, Z., Zou, W.-L., Fan, K.-W., Zhang, J., Rahardjo, H., Fredlund, D. G. 2022. Influences of temperature and moisture fluctuations on soil shrinkage and water retention curves of compacted expansive soils. Engineering Geology, 306, 106533. https://doi.org/10.1016/j.enggeo.2022.106533

Henke, S., Vogel, A., Reiswig, K. 2023. Untersuchungen zum Schrumpfverhalten bindiger Böden unter Nutzung von 3D-Laserscanning.

Ivoke, J., Khan, M. S., et al. 2021. Unsaturated hydraulic conductivity variation measurements in expansive clay during seasonal fluctuations. Transportation Research Record, 2675(11), 663–673. https://doi.org/10.1177/03611981211011994

Izdebska-Mucha, D., Wójcik, E. 2013. Testing shrinkage factors: Comparison of methods and correlation with index properties of soils. Bulletin of Engineering Geology and the Environment, 72(1), 15–24. https://doi.org/10.1007/s10064-012-0449-0

Jain, S., Wang, Y. H., Fredlund, D. G. 2015. Non-contact sensing system to measure specimen volume during shrinkage test. Geotechnical Testing Journal, 38(4), 403–412. https://doi.org/10.1520/GTJ20140274

Janga, J. K., Reddy, K. R., Schulenberg, J. 2024. Climate change impacts on safety of levees: A review / Impacts du changement climatique sur la securité des digues: un examen. Proceedings of the ECSMGE 2024. https://doi.org/10.1201/9781003431749-310

Kutter, B. L. 2013. Effects of capillary number, Bond number, and gas solubility on water saturation of sand specimens. Canadian Geotechnical Journal, 50(2), 133–144. https://doi.org/10.1139/cgj-2011-0250

Lin, L. C., Benson, C. H. 2000. Effect of wet–dry cycling on swelling and hydraulic conductivity of GCLs. Journal of Geotechnical and Geoenvironmental Engineering, 126(1), 40–49. https://doi.org/10.1061/(ASCE)1090-0241(2000)126:1(40)

Louati, F., Trabelsi, H., Mehrez, J., et al. 2018. Wet–dry cycles effect on the saturated hydraulic conductivity. https://doi.org/10.1080/19648189.2018.1541144

Lu, H., Liu, J., Li, Y., Dong, Y. 2015. Heat transport and water permeability during cracking of the landfill compacted clay cover. International Journal of Geophysics, 2015, 786419. https://doi.org/10.1155/2015/786419

Malusis, M. A., Yeom, S., Evans, J. C. 2011. Hydraulic conductivity of model soil–bentonite backfills subjected to wet–dry cycling. Canadian Geotechnical Journal, 48(8), 1198–1211. https://doi.org/10.1139/T10-098

Mitchell, A. R. 1991. Soil surface shrinkage to estimate profile soil water. Irrigation Science, 12(1), 1–6. https://doi.org/10.1007/BF00190569

Peng, X., Horn, R. 2007. Anisotropic shrinkage and swelling of some organic and inorganic soils. European Journal of Soil Science, 58(1), 98–107. https://doi.org/10.1111/j.1365-2389.2006.00808.x

Peng, X., Horn, R. 2013. Identifying six types of soil shrinkage curves from a large set of experimental data. Soil Science Society of America Journal, 77(2), 377–386. https://doi.org/10.2136/sssaj2011.0422

Puppala, A., Cerato, A. 2009. Heave distress problems in chemically-treated sulfate-laden materials.

Rao, K. S. S., Rao, S. M., Gangadhara, S. 2001. The impact of cyclic wetting and drying on the swelling behaviour of stabilized expansive soils. Engineering Geology, 60(3–4), 223–233. https://doi.org/10.1016/S0013-7952(00)00089-3

Romero, E., Simms, P. H. 2008. Microstructure investigation in unsaturated soils: A review with special attention to contribution of mercury intrusion porosimetry and environmental scanning electron microscopy. Geotechnical and Geological Engineering, 26, 705–727. https://doi.org/10.1007/s10706-008-9204-5

Sander, T., Gerke, H. H. 2007. Noncontact shrinkage curve determination for soil clods and aggregates by three-dimensional optical scanning. Soil Science Society of America Journal, 71(5), 1448–1451. https://doi.org/10.2136/sssaj2006.0372

Schultze, E., Muhs, H. 1967. Bodenuntersuchungen für Ingenieurbauten. Berlin: Springer-Verlag.

Sharanya, A. G., Mudavath, H., Thyagaraj, T. 2021. Review of methods for predicting soil volume change induced by shrinkage. Innovative Infrastructure Solutions, 6, 130. https://doi.org/10.1007/s41062-021-00485-1

Spillecke, L., Knut, A., Bornschein, A., Thiel, R., Wasner, L., Knöcher, S. 2025. Automated determination of the soil shrinkage limit and potentials of the soil shrinkage curve, measured by multiple continuous optical methods. Accepted.

Tang, C.-S., Zhu, C., Cheng, Q., Zeng, H., Xu, J.-J., Tian, B.-G., Shi, B. 2021. Desiccation cracking of soils: A review of investigation approaches, underlying mechanisms, and influencing factors. Earth-Science Reviews, 216, 103586. https://doi.org/10.1016/j.earscirev.2021.103586

Van Genuchten, M. Th. 1980. A closed-form equation for predicting the hydraulic conductivity of unsaturated soils. Soil Science Society of America Journal, 44(5), 892–898. https://doi.org/10.2136/sssaj1980.03615995004400050002x

Vogt, N., Birle, E., Heyer, D., Etz, A. 2013. Entwicklung einer neuen Versuchstechnik zur Bestimmung der Grenze zwischen halbfestem und festem Boden. Bergisch Gladbach: Bundesanstalt für Straßenwesen Straßenbau. ISBN: 9783956060106

Wong, J. M., Elwood, D., Fredlund, D. G. 2019. Use of a three-dimensional scanner for shrinkage curve tests. Canadian Geotechnical Journal, 56(1), 125–132. https://doi.org/10.1139/cgj-2017-0700

Yan, F., Fu, Y., Tall, A., Zhang, F., Arthur, E. 2022. Coefficient of linear extensibility of soil can be estimated from hygroscopic water content or clay and organic carbon contents. European Journal of Soil Science, 73(3), e13298. https://doi.org/10.1111/ejss.13298

Zhou, A.-N., Sheng, D., Carter, J. P. 2012. Modelling the effect of initial density on soil-water characteristic curves. Géotechnique, 62(8), 669–680. https://doi.org/10.1680/geot.10.P.120